New Directions in Earth Observing: Scientific Applications of Multiangle Remote Sensing

David J. Diner,* Gregory P. Asner,+ Roger Davies,# Yuri Knyazikhin,@ Jan-Peter Muller,& Anne W. Nolin,** Bernard Pinty,## Crystal B. Schaaf,@ and Julienne Stroeve**

ABSTRACT

The physical interpretation of simultaneous multiangle observations represents a relatively new approach to remote sensing of terrestrial geophysical and biophysical parameters. Multiangle measurements enable retrieval of physical scene characteristics, such as aerosol type, cloud morphology and height, and land cover (e.g., vegetation canopy type), providing improved albedo accuracies as well as compositional, morphological, and structural information that facilitates addressing many key climate, environmental, and ecological issues. While multiangle data from wide field-of-view scanners have traditionally been used to build up directional "signatures" of terrestrial scenes through multitemporal compositing, these approaches either treat the multiangle variation as a problem requiring correction or normalization or invoke statistical assumptions that may not apply to specific scenes. With the advent of a new generation of global imaging spectroradiometers capable of acquiring simultaneous visible/near-IR multiangle observations, namely, the Along-Track Scanning Radiometer-2, the Polarization and Directionality of the Earth's Reflectances instrument, and the Multiangle Imaging SpectroRadiometer, both qualitatively new approaches as well as quantitative improvements in accuracy are achievable that exploit the multiangle signals as unique and rich sources of diagnostic information. This paper discusses several applications of this technique to scientific problems in terrestrial atmospheric and surface geophysics and biophysics.

1. Introduction

With the exception of the mirrorlike surface of an absolutely calm body of water, all natural terrestrial surfaces and media reflect light diffusely. Clouds, aerosol layers, vegetation canopies, soils, snow fields—all scatter shortwave radiation into an angular reflectance pattern or Bidirectional Reflectance Distribution Function (BRDF) (Nicodemus et al. 1977) whose magnitude and angular shape is governed by the composition, density, and geometric structure of the reflecting medium. In practical terms, the BRDF is the directional radiance reflected from a target, divided by the irradiance (incident flux) illuminating the target at a single incidence angle. It is widely accepted that the assumption of Lambertian, or directionally isotropic, BRDF is not valid (Kimes et al. 1987; Privette et al. 1997a). Developments in remote sensing technology and radiative transfer modeling indicate that angular (also referred to as directional or goniometric) signatures can be measured and exploited to provide not only improved accuracies relative to single-angle approaches but also unique diagnostic information about the earth's atmosphere and surface, capitalizing on both the geometric aspects of the technique (e.g., through the use of stereophotogrammetic cloud height retrievals, wind retrievals, and cloud detection) as well as the radiometric variations in signal with angle (e.g., for identification of atmospheric aerosol, cloud, or surface vegetation type). In this paper we illustrate how a number of scientific

*Jet Propulsion Laboratory, California Institute of Technology, Pasadena, California.
+Stanford University, Stanford, California.
#The University of Arizona, Tucson, Arizona.
@Boston University, Boston, Massachusetts.
&University College London, London, United Kingdom.
**University of Colorado, Boulder, Colorado.
##Joint Research Centre, Ispra, Italy.
Corresponding author address: David J. Diner, JPL Mail Stop 169-237, 4800 Oak Drive, Pasadena, CA 91109.
E-mail: djd@jord.jpl.nasa.gov
In final form 19 May 1999.

applications benefit explicitly from the acquisition of multiangle data.

Traditionally, remote sensing approaches using wide field-of-view scanners such as the Advanced Very High Resolution Radiometer (AVHRR) have often considered the view angle and solar zenith angle dependence of reflected radiation to be a problematic source of noise or error, requiring a correction or normalization to a "standard" (e.g., nadir) direction. The Earth Radiation Budget Experiment (ERBE) scanners, currently supplanted by the Clouds and the Earth's Radiant Energy System (CERES) scanners (Wielicki et al. 1996), measure the directionality of given scene types (e.g., cloud-free land, stratus clouds) by building up angular reflectance signatures over time in a statistical sense. In the ERBE/CERES case, these patterns are used to convert point measurements of radiance to albedos. This "sequential" multiangle concept has been applied successfully to conventional meteorological sensors (Li et al. 1996; Cabot and Dedieu 1997; d'Entremont et al. 1999) and will be used with the Earth Observing System Moderate-resolution Imaging Spectroradiometer (MODIS) (Wanner et al. 1997; Lucht et al. 1999). However, many weeks are typically required to construct the directional patterns, during which time changes in either the surface or atmosphere can contribute a significant source of noise to the characterization of the scene or, in the most dynamic cases (e.g., clouds), render instantaneous identification of the physical scene state impossible.

Advances in remote sensing technology, for example, array detectors allowing the construction of compact sensors, now facilitate the more difficult challenge of acquiring, on a global basis, "simultaneous" multiangle measurements of the reflected radiation from individual scenes, with spatial resolutions ranging from several kilometers to a few hundred meters. A major attribute of this approach is its amenability to using the directionality itself for instantaneous scene identification and characterization, enabling the incorporation of physical modeling into the data interpretation with attendant increases in accuracy and information content. We define simultaneous multiangle observing as the acquisition of measurements at more than one angle in an orientation along the flight direction of the remote sensing platform (see Fig. 1). Admittedly, this does not precisely represent "true" simultaneity, which would require multiple, widely spaced platforms. However, with the exception of wind-driven clouds, most natural scenes are relatively static over the several minutes required for an aftward- or nadir-viewing sensor to acquire the same target that was previously observed by a forward-viewing sensor on the same spacecraft. In the case of clouds, the small departure from true simultaneity can be turned to advantage, enabling retrieval of cloud velocities.

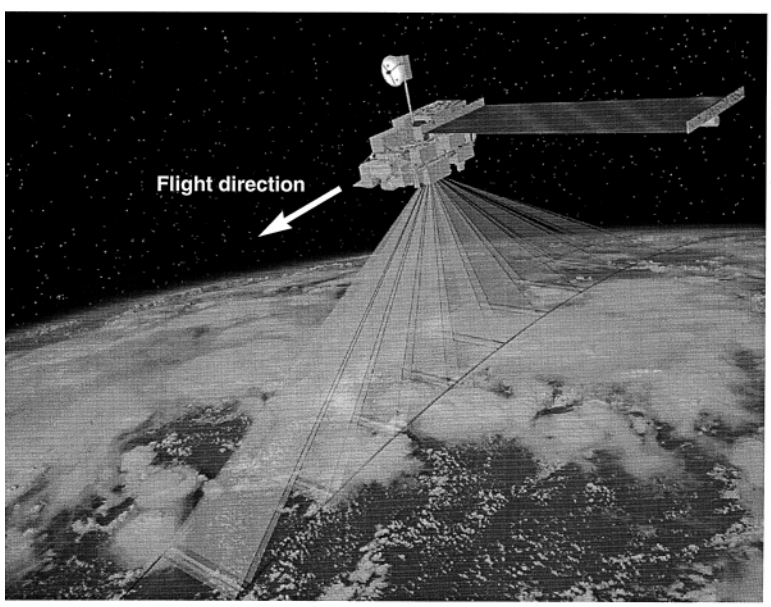

FIG. 1. The concept of "simultaneous" multiangle imaging is illustrated using the example of MISR aboard the Terra spacecraft. Forward motion of the spacecraft causes points on the ground to be observed in turn by the nine pushbroom cameras that are oriented at fixed along-track view angles. ATSR-2 uses a conical scan to acquire data in similar fashion but at two angles, one forward oblique angle plus nadir. POLDER uses an area array and a wide angle lens, so imagery at intervening angles to that shown in this diagram is obtained. Each of these instruments depends on forward motion of the spacecraft to obtain images of a specific ground target at multiple angles.

Several instruments designed specifically for multiangle observation at visible and shortwave infrared wavelengths have already acquired global data from space or will be doing so in the near future. The Along-Track Scanning Radiometer-2 (ATSR-2) was launched in April 1995 aboard the European Remote Sensing satellite *ERS-2*. It consists of a conical scanning radiometer that provides curved swaths at two measurement angles, one near nadir and the other at an oblique forward-viewing angle. The Polarization and Directionality of the Earth's Reflectances (POLDER) instrument aboard the Japanese Advanced

Earth Observing Satellite (ADEOS) acquired eight months of data between November 1996 and June 1997 and a follow-on instrument is planned for launch aboard *ADEOS-2* in mid-2000. POLDER uses a wide-angle imaging system and an area array detector to acquire measurements at a multitude of along-track and cross-track angles. The Multiangle Imaging SpectroRadiometer (MISR) is planned for launch aboard the Earth Observing System Terra (formerly EOS AM-1) spacecraft in summer 1999. The MISR instrument uses nine separate pushbroom cameras to acquire data at nine discrete along-track observation angles. A comparison of the observational characteristics of these three instruments is provided in Table 1. For any specific application, the attributes (e.g., number of angles, calibration accuracy, ground footprint, signal-to-noise ratio) must be considered together in determining what constitutes the most suitable approach. Information on ATSR-2 was taken from Stricker et al. (1995) and Koelemeijer et al. (1998); on POLDER from Deschamps et al. (1994) and Hautecoeur and Leroy (1998); and on MISR from Diner et al. (1998a).

Example angular reflectance patterns are shown in Fig. 2, which shows top-of-atmosphere 672-nm bidirectional reflectance factor (BRF) measurements acquired at nine discrete view angles by the Airborne Multiangle Imaging SpectroRadiometer (AirMISR), a pushbroom imager utilizing a single camera in a pivoting gimbal mount (Diner et al. 1998b). The BRF is a dimensionless quantity equal to the directional radiance reflected from a target that is illuminated by a source at a single incidence angle, divided by the radiance that would have been reflected under the same illumination conditions by a perfect lambertian reflector. Numerically, the BRF is equal to π steradians times the BRDF. The AirMISR camera was constructed from spare optical and focal plane assemblies provided by the MISR project and has similar performance characteristics to the MISR cameras except that flight at 20-km altitude yields a swath width of about 10 km and footprints that are resampled and map-projected to 27.5 m at all angles. The measurements represent averages over a 138 m $\times$ 138 m vegetated (grassy) area (the Brookside Golf Course near the Rose Bowl in Pasadena, California, acquired on 5 December 1998); a 1.1 km $\times$ 1.1 km urban scene (streets and buildings in Pasadena, from the same imagery); a 1.1 km $\times$ 1.1 km area from Rogers Dry Lake in the Mojave Desert, California (acquired on 11 December 1998); and a 1.1 km $\times$ 1.1 km area of a stratus cloud (acquired during the Arctic Cloud Experiment over Alaska on 3 June 1998). For the land surface scenes, the aerosol loading was determined using sunphotometry to be very low (optical depth < 0.02 at 670 nm)

TABLE 1. Comparison of the ATSR-2, POLDER, and MISR instruments.

Parameter	ATSR-2	POLDER	MISR
Number of along-track view angles	2	Up to 14	9
Maximum view angle (at earth's surface)	56° (forward only)	60° (forward + aftward)	70.5° (forward + aftward)
Time interval between most extreme views	2 min	4 min	7 min
Shortwave spectral bands	555, 659, 865, 1600 nm	443, 490, 565, 670, 763, 765, 865, 910 nm	446, 558, 672, 866 nm
Footprint (nadir)	1×1 km^2	6×7 km^2	275×275 m^2; 1.1×1.1 km^2
Swath width	512 km	2200 km	360 km
Quantization	10 bits	12 bits	14 bits, square-root encoded to 12 bits
Onboard calibration	Yes	No	Yes

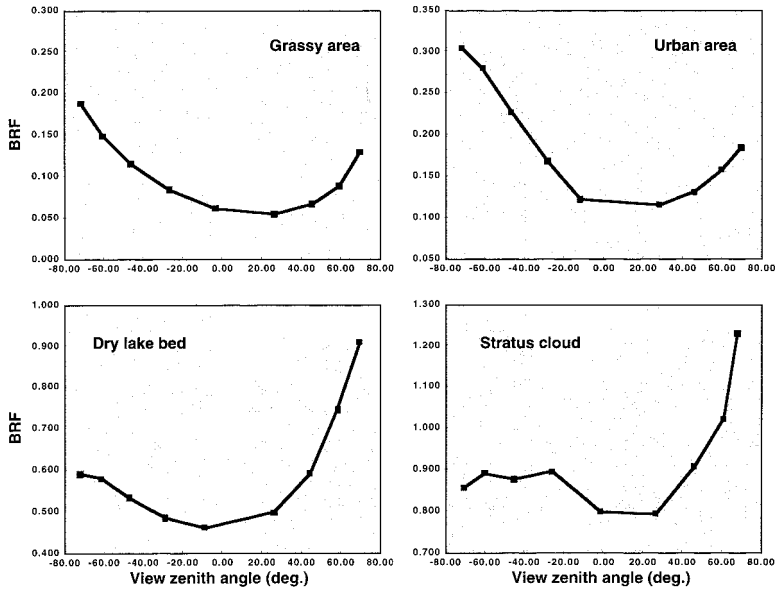

FIG. 2. Top-of-atmosphere BRF measurements acquired by AirMISR. Scene descriptions are provided in the text. View zenith angles are shown with a positive (negative) sign if the measurements correspond to forward (backward) scattering. All observations were acquired at solar zenith angles 57°–58°. Scattering angles ranged from a low of about 53° to a high of about 168°. AirMISR uses a single, gimballed camera to acquire multiangle images of selected ground targets by first taking data while fixed at the most forward angle, then stepping to the next angle to reacquire the target at the next angle, and so on. Obtaining a continuous swath of multiangle data requires an approach more like that used by MISR, ATSR-2, or POLDER.

and thus the BRF's are predominantly governed by the surface characteristics. Lidar and AirMISR stereoscopic retrievals put the stratus cloud top at an altitude of about 3 km (Moroney et al. 1999) and the cloud optical depth, estimated from lidar and microwave radiometer data, was around 10 (Várnai et al. 1999). The data show the grass and urban targets to be more strongly backscattering, presumably due to the greater geometric area covered by shadows in the forward-scattering views. On the other hand, the relatively homogeneous dry lake bed and stratus cloud scenes, composed of optically thick particulate media, are predominantly forward scattering as a result of scattering by the constituent particles.

2. Applications

The efficacy of any remote sensing technique must be measured against its ability to address important scientific objectives. Therefore, we have formulated our discussion of multiangle remote sensing by posing a series of science questions to which such data bring unique or more accurate information relative to single-angle methods. Direct answers to these questions are beyond the scope of not only this paper but the current state of knowledge; however, we use them as a framework to elucidate how multiangle data benefit the particular topic, to discuss relevant attributes of the multiangle measurements, and to provide quantitative examples of the positive impact of incorporating such data. Our discussion concentrates on four areas: cloud radiative forcing, aerosol climatic effects, cryosphere–climate interdependencies, and land vegetation–atmosphere interactions.

a. Cloud radiative forcing

What is the magnitude of cloud radiative forcing as a function of cloud type? The earth's climate is strongly affected by clouds, and even small systematic changes in their presence or properties can have a highly significant effect on the climate system (Arking 1991). Uncertainty regarding the magnitude and nature of cloud effects is a very well-recognized limitation to the more general problem of predicting future climate change (IPCC 1995a). In the future, cloud properties are expected to change in response to at least three possible influences: changes in cloud condensation nuclei due to anthropogenic aerosol sources near the surface affecting the albedo of lower tropospheric clouds; changes in ice nuclei concentration affecting cirrus cloud presence and optical depth due to aircraft emissions in the upper troposphere; and as a natural response of the system to changes in temperature, water vapor, and heat transport associated with global warming. Also, if the relative magnitudes of vertical and horizontal heat transport change in response to global warming, there should be an associated change in the relative frequency of cumuliform versus stratiform cloud types. That is, cloud morphologies may change in addition to their microphysical properties, with correspondingly large effects on radiative fluxes.

A frequently used starting point in studies of the shortwave effects of clouds on the climate system is the shortwave cloud radiative forcing at the top of the atmosphere. This is the difference between the average absorbed (i.e., incident minus reflected) solar ir-

radiance, over a given region and time, and the component of this average attributable to clear sky conditions only. To obtain an accurate measure of this forcing it is necessary to correctly estimate both the bidirectional properties of all scene types as well as the subset of the measurements that are strictly cloud free. Simultaneous multiangle measurements improve both of these estimates relative to what is possible from single-angle views, and also permit expanded studies of forcing as a function of cloud type.

We first consider the determination of cloud albedo as a function of cloud type. Cloud albedo is an essential ingredient for equilibrium climate models that are used to assess the global role of clouds. Globally, the average shortwave cloud radiative forcing is roughly -50 W m^{-2} (Ramanathan et al. 1989). An uncertainty in average cloud albedo of only 0.02 (corresponding to an uncertainty in planetary albedo of 0.01) is sufficient to mask the entire longwave radiative forcing due to a doubling of CO_2, all other factors remaining constant. With multiangle measurements, the shortwave forcing can be determined more accurately, and better related to different cloud regimes. This information can, in turn, be applied to climate models to better understand the complex role of cloud shortwave forcing.

The determination of cloud albedo from radiance measurements inevitably requires the use of some sort of bidirectional cloud model. ERBE, for example, used a stochastic summary (Smith et al. 1986) of past measurements to determine a bidirectional model that was loosely dependent on cloud amount, but not on cloud properties. Unfortunately, since the bidirectional model and cloud albedo tend to be correlated, it is hard to achieve high accuracy with such a technique. Thick clouds with high albedos tend to reflect more isotropically than do thin clouds with low albedos, provided both types meet the one-dimensional idealization of being plane parallel. Most, if not all, clouds depart externally or internally from this idealization, however, resulting in significantly different anisotropic reflectivity when compared to one-dimensional models. Single-angle views have great difficulty in choosing the correct cloud model because they cannot distinguish the many degrees of freedom defining cloud shape. Simultaneous multiangle measurements improve this situation in two ways: by making more measurements at different angles, the angular integration of the radiance field over the full hemisphere is estimated more accurately; and by providing more information on scene anisotropy a better model can be used to fill in the missing directions. Issues here involve accounting for the asymmetry between forward and aftward bidirectional reflection, extrapolation to more oblique viewing angles, and correcting for azimuthal variations in the bidirectional reflection function. Davies and Várnai (1997) have simulated these effects for a wide variety of modeled cloud scenes, including both horizontally homogeneous and heterogeneous cloud types. An example of the albedo errors they found using different retrieval techniques is shown in Fig. 3. The figure contrasts albedo errors from single- and multiangle views expected for three different estimation techniques: numerical extrapolation over the hemisphere with no model input; use of a stochastically generated generic cloud model; and use of specific cloud models that best match the measured radiances. The single-angle view is taken to be the nadir direction, and the multiangle views are the nine MISR viewing angles. All of these errors rise with increasing solar zenith angle, which is 60° for this example. The general conclusion of Davies and Várnai (1997) is that in going from a single viewing direction to nine multiple directions, increased angular sampling reduces the albedo error by about a factor of three, and the improved ability to use a better estimation technique further reduces the error by an additional factor of three. Overall, there should thus be an order of magnitude improvement in the accuracy of

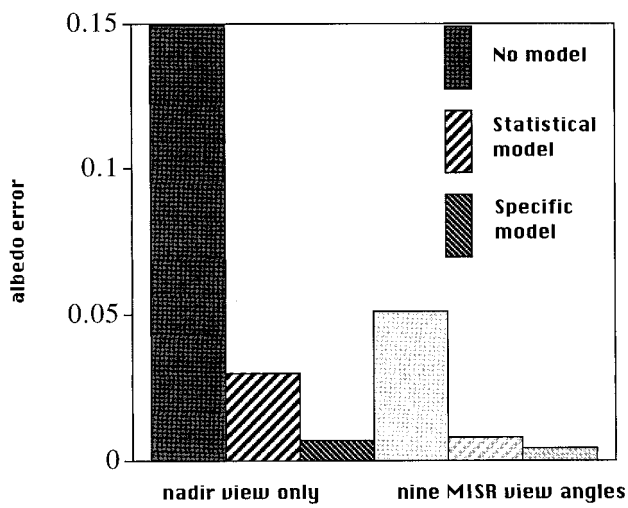

FIG. 3. Typical errors in narrowband visible albedo estimates using different methods, adapted from Davies and Várnai (1997). The left-hand set of columns refers to a single-angle measurement in the nadir direction, and the right-hand set to multiangle measurements at the MISR view angles. Solar zenith angle is 60°. Results are root-mean-square errors in the albedos of ~100 different types of cloud field models, including both heterogeneous and homogeneous scenes.

individual scene albedos when nine multiangle measurements are made, compared to single-angle views.

Associated with improvements in the albedo of individual scenes, multiangle viewing also provides useful information about the scene type. One example is the application of stereo techniques to retrieve cloud top heights (Hasler 1981; Lorenz 1985) independent of assumptions about the atmospheric thermal structure. These heights are required in order to register the multiangle measurements to a common surface for albedo determinations, and are useful in determining some cloud characteristics. For example, stereoscopic retrieval of cloud height over snow or other high albedo surfaces is a very useful technique simply for detecting the presence of a cloud that might be impossible to detect using a brightness threshold. In polar regions, the net radiative impact of clouds is still uncertain (Charlock and Ramanathan 1985; Li and Leighton 1991). Some studies indicate that clouds tend to warm the surface–atmosphere system over highly reflective surfaces (Stephens et al. 1981; Nakamura and Oort 1988) and other studies indicate that clouds have a net cooling effect (Li and Leighton 1991; Schweiger and Key 1994). One of the reasons for this uncertainty is that scene identification and cloud detection remain difficult over snow- and ice-covered surfaces. An evaluation of stereoscopic cloud detection over Greenland using MISR algorithms applied to ATSR-2 data (Muller et al. 1999, unpublished manuscript) indicates that this method provides a more robust separation of cloud from snow than radiance-based thresholding (Cawkwell et al. 1999, unpublished manuscript).

In principle, only two angles are needed for a stereo height retrieval, providing either a conventional cloud classifier (low, middle, and high), or a quantitative classification by the actual height retrieved. However, views from more than two angles not only improve the confidence of the cloud top height determination, but also allow additional features to be retrieved. For example, measurements of a given scene with three or more views made at the slightly different times during an orbital pass can be used to unscramble the effects of wind advection from those of height on the apparent disparities (Diner et al. 1997a). Also, the aspect ratio of clouds may at times be retrievable in those cases where there is a cloud base that is visible from space, using the asymmetry between forward and aft viewing measurements of disparity. This should allow a distinction between stratiform and cumuliform cloud morphologies.

Besides stereo, multiangle radiance measurements enable other techniques to detect and classify cloudy scenes. The application of angular signatures to cloud remote sensing was first introduced by Di Girolamo and Davies (1994), who developed the Band Differenced Angular Signature as a means of detecting thin cirrus. Using simulated data, they showed that cirrus with visible optical depths as low as 0.5 should be detectable by MISR even without a priori knowledge about the underlying scene characteristics. This technique is based on the obscuration of the angular signature of the Rayleigh scattering component when high cloud is present, and even permits the detection of thin cirrus in the presence of low level cloud. Angular signatures of different cloud types are also possible based on statistical summaries of the gray level difference vector as a function of angle. These are information summarizing techniques that require some initial training based on characteristics of known cloud fields.

The information gained about scene type using multiangle views naturally includes the detection of clear sky events, needed to complete the measurement of cloud radiative forcing so that the clear sky component can be subtracted from the total. Clear sky events are already routinely recorded with some success in the form of composited clear sky radiance maps from single-angle meteorological satellite imager data using automated approaches such as AVHRR Processing scheme Over cloud Land and Ocean (APOLLO) (Saunders and Kriebel 1988; Gesell 1989), Clouds from AVHRR (CLAVR) (Stowe et al. 1991, 1994), Support of Environmental Requirements for Cloud Analysis and Archive (SERCAA) (Gustafson et al. 1994), and International Satellite Cloud Climatology Project (ISCCP) (Rossow and Gardner 1993a,b). These methods work, by and large, through a comparison of the instantaneous measured radiance with a database of previously observed radiances over given surface types, using fixed or dynamic thresholding techniques. Similar methods will be used with MODIS (Ackerman etal. 1998), CERES (Baum et al. 1995), and MISR (Diner et al. 1997b). In the latter case, simultaneous multiangle measurements will offer some benefit because of the greater confidence that comes from having more independent measurements of the same scene, since the thresholds are angle dependent and would have to be satisfied simultaneously at all viewing angles for the scene to be classified as clear. The global anisotropic information required to improve the modeling and monitoring of clear sky

radiance data from meteorological sensors could be routinely provided by multiangle sensors flying concurrently with the next-generation meteorological satellites (the National Polar Orbiting Environmental Satellite System, NPOESS). Perhaps the biggest advantage of the multiangle approach will come from the ability to differentiate clear skies from scenes containing thin cirrus or containing clouds over snow.

b. Aerosol climatic effects

What is the spatial and temporal distribution of atmospheric aerosol abundance and type, and what is their effect on climate? Aerosols are solid or liquid airborne particulates of various compositions, frequently found in stratified layers. In the troposphere, they arise from natural sources, such as dust storms, desert and soil erosion, biogenic emissions, forest and grassland fires, and sea spray, as well as anthropogenic activity—for example, industrial pollution. In addition to their potential indirect effect on climate described in section 2a, they play a direct role in the radiation budget of earth, on regional and hemispheric length scales (Charlson et al. 1992; Kiehl and Briegleb 1993), and are thought to produce, on average, a net global cooling effect. Northern Hemispheric sources are believed to be sufficiently large so that the net radiative effect of anthropogenic sulfate aerosols alone is comparable in size (of order 1–2 W m^{-2}), though opposite in sign, to the anthropogenic CO_2 radiative forcing (Charlson et al. 1991), but the magnitude of this is very uncertain. The potential climatic impact of aerosols is more significant than a simple offset to the magnitude of global warming (IPCC 1995a). The lifetimes of tropospheric aerosol particles are short (weeks) relative to global atmospheric mixing times, the sources are spatially and temporally heterogeneous, and the magnitude and sign of their net radiative effect depends on their optical properties and the albedo of the underlying surface. Thus, aerosols can also affect atmospheric heating in a spatially heterogeneous manner that can influence regional energy budgets and possibly precipitation patterns in ways that are presently poorly understood.

Multiangle viewing provides information about aerosols in two principal ways. First, the oblique viewing angles accentuate the aerosol signal because of the increased optical path length through the atmosphere, and second, the method provides coverage in scattering angle (the angle between the direction of the sun's rays and the direction to the sensor), enabling distinguishability of aerosol types of varying compositions and sizes. Due to the highly variable nature of aerosol composition, application of multiangle aerosol retrieval methods require data collected with near simultaneity. Current operational aerosol retrievals over ocean from AVHRR (Husar et al. 1997; Stowe et al. 1997) do not distinguish different particle types or compositions since they are based on measurements at a single wavelength and angle of view, and the algorithm to convert observed radiance to aerosol optical depth assumes spherical particles with complex refractive index $n = 1.5 - 0.0i$ ("sulfate" composition), a specific Junge distribution of sizes, and an assumed Lambertian surface reflectivity. Although a provisional identification of aerosol type can be made from an analysis of the spatial and temporal context (e.g., windblown desert dust from Africa and Asia) (Husar et al. 1997), a more objective and automated identification method is needed to systematically retrieve the optical depths and optical properties with accuracies required for climate modeling. For example, Mishchenko et al. (1995) point out that satellite-retrieved optical depth errors for nonspherical dust aerosols can exceed 100% if the particles are assumed to be spherical. Aerosol optical depth errors also result from the assumption of incorrect size distributions or refractive indices (Wang and Gordon 1994). Consequently, the remote sensing technique must be able to distinguish between different aerosol types in retrieving optical depths.

The difficulty with single view angle observations is that the problem is severely underconstrained: at any single angle, the optical depth can always be adjusted to give an equivalent radiance for different aerosol types. An example of this is shown in Fig. 4. This example makes use of simulated MISR observations over a black surface (an approximation to a deep, calm water body away from the specular direction), and shows the retrieval results obtained as a function of optical depth for the case in which the "true" aerosol is composed of soot particles and the "assumed" aerosol for the purpose of the retrieval is accumulation mode sulfate. The sun angle is 45.6° and the assumed observation date is 21 March. The reduced χ^2 parameters are weighted sums of the squares of the differences between model and simulated measurement values, normalized by the estimated measurement uncertainty and the number of measurements. Large χ^2 indicates distinguishability, whereas small χ^2 indicates indistinguishability between an assumed model and the measurements. Formally, values of χ^2 in the range 1–2 correspond to confidence between about

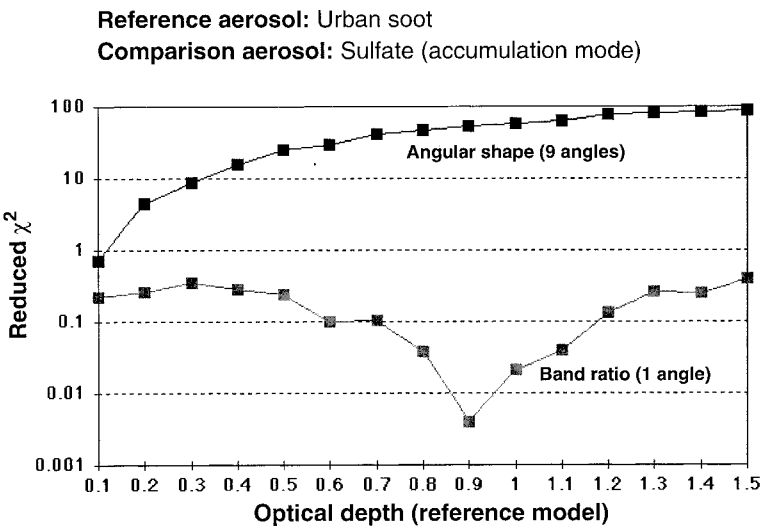

FIG. 4. Theoretical comparison of the distinguishability of two different aerosol types over a dark surface using single-angle vs multiangle data. The inability of the nadir view to distinguish between a soot and sulfate aerosol, indicated by reduced $\chi^2 < 1$ (see text), will result in a highly inaccurate retrieval of optical depth. The multiangle data are able to identify that an incorrect aerosol model has been assumed.

55% and 99% that an incorrect model has not been accepted. For the simulated nadir observation, the curve labeled "Band ratio (1 angle)" makes use of the ratio of nadir radiances in the near-infrared (NIR) and red. The nine-angle simulation uses the MISR view angles, corresponding to scattering angles varying from about 73° to 140° at the prescribed orbital and illumination conditions. Here, the curve labeled "Angular shape (9 angles)" represents reduced χ^2 values for the difference between model and simulated measured off-nadir/nadir radiance ratios in the red band, summed over all view angles. In each case, the selected metric provided the best distinguishability. In both the nadir and multiangle simulations, the optical depth that minimized the residuals between the model and simulated measured red band radiances was used to calculate the reduced χ^2 values. Because of the large difference in single scattering albedo for the soot and sulfate aerosols, the best-fitting optical depths differed from the correct values by more than a factor of 5 at unit optical depth; however, in the nadir case the observational indistinguishability of the aerosol signals means that there is insufficient information to know that the incorrect optical depth has been retrieved. In the multiangle case, the large values of χ^2 would cause the incorrect comparison aerosol model type to be rejected (except, in this particular example, at optical depths < 0.1). Further information on the use of such reduced χ^2 metrics for aerosol retrieval, and sensitivity of multiangle observations to optical depth, particle size, particle shape, and composition may be found in Kahn et al. (1997, 1998). Regardless of aerosol type, as long as the particles are not too absorbing (imaginary refractive index < 0.008), optical depth uncertainties of 0.05 or 20% (whichever is larger) are predicted (Kahn et al. 1998).

Over land the indeterminate nature of the retrievals using remote sensing data is exacerbated relative to the ocean case because the surface bidirectional reflectance is an additional and highly variable free parameter. As a consequence, separation of the land-leaving and atmosphere-leaving signals in remotely sensed radiances must be performed in order to retrieve aerosol properties from the measured signal. A number of approaches making explicit use of multiangle observations have been developed. One makes use of expected differences in the nature of multiangle signal variation between the surface and atmosphere, in particular, the spectral invariance in the shape of the surface bidirectional reflectance at selected wavelengths; this approach is currently being tested and validated using ATSR-2 data over the Tropospheric Aerosol Radiative Forcing Observational Experiment (TARFOX) (Veefkind et al. 1998) and over the Boreal Ecosystem–Atmosphere Study (BOREAS) area in Canada (North 1998), and is also being developed as a method for reprocessing of daily aggregated multiangle Meteosat data for the coupled retrieval of surface albedo and effective aerosol optical depth (Pinty et al. 1998a). The latter is an extension to broader land surface classes of the method used over dense, dark vegetation as part of the MISR aerosol retrieval algorithm (Martonchik et al. 1998a). Separability of the surface-leaving and atmosphere-leaving signals over terrain with heterogeneous surface reflectance is another multiangle land aerosol retrieval method used by MISR (Martonchik and Diner 1992; Martonchik et al. 1998a). This method models the shape of the surface bidirectional reflectance as a linear sum of empirical orthogonal angular functions derived directly from the image data, making use of spatial contrasts to separate the surface and atmospheric signals. These techniques for aerosol retrieval over land are uniquely facilitated by the acqui-

sition of multiangle data and are unavailable to single-angle observations.

The determination of aerosol optical properties over land is also an essential prerequisite to accurate retrievals of clear (noncloudy) surface reflectance factors and albedos. Such retrievals require an algorithm that incorporates an appropriate surface BRDF model (Tanre et al. 1983; Lee and Kaufman 1986; Vermote et al. 1997a,b; Martonchik et al. 1998b). Studies have shown that methods relying on a Lambertian surface assumption result in mean errors of 2%–7% over corrections that include surface BRDF effects (Hu et al. 1999; Vermote et al. 1997a). Accurate atmospheric modeling and surface retrieval are particularly key in validation exercises where attempts are made to tie satellite (or airborne) observations to ground-based measurements or in mesoscale field studies where surface observations are coupled with remotely sensed data.

c. Cryosphere–climate interdependencies

How stable is the cryosphere relative to climate change, and conversely, how does the climate respond to changes in the cryosphere? With the recognition that cryospheric variations accompany large-scale atmospheric and oceanic circulation anomalies on several timescales, the cryosphere is considered an extremely important component of our climate system. Its importance results mainly from its high albedo, low thermal conductivity, and high interseasonal variability. Snow surfaces have albedos that often exceed 90% in the visible part of the spectrum (Warren 1982), making snow the brightest common land cover type on Earth. Small decreases in albedo, either due to a reduction in snow- and ice-covered area or as a result of snow grain growth, can easily double the amount of energy absorbed by the snowpack (Nolin and Stroeve 1997; Stroeve et al. 1997). Oerlemans and Hoogendoorn (1989) showed that the surface albedo is the most critical parameter in modeling the change in mass balance of glaciers. Model results by Maykut and Untersteiner (1971) indicated a complete disappearance of perennial Arctic sea ice for a 15% to 20% decrease in the summer albedo. During summer months on the ice sheets, increased solar radiation leads to surface warming, snow grain growth, and in some areas, surface melt. Both grain growth and melt result in decreased surface albedo leading to further solar absorption and warming. This positive feedback is a seasonal process but may also occur over much longer timescales. Because of the climatological interest of the heat balance of sea ice, ice sheets, and snow-covered areas, there is a need for large-scale spatial and temporal measurements of the snow/ice albedo.

Recent work in Greenland and Antarctica has demonstrated that the surface albedo is also important in determining the cloud radiative forcing (Bintanja and Van den Broeke 1996). The balance between shortwave and longwave radiation at the surface determines whether clouds will have a cooling or warming effect. Thin clouds increase surface net radiation because they transmit substantial shortwave energy to the surface and also enhance longwave input. Multiple shortwave reflections from clouds are responsible for increased solar insolation at the snow surface, so thin clouds over a bright surface lead to an increase in both shortwave and longwave contributions. To shift the radiation balance, the cloud albedo must increase (via increasing optical thickness) to reduce the shortwave radiation at the surface. The brighter the ice sheet (higher the surface albedo), the greater the cloud optical depth must be in order to have a surface cooling effect.

Looking beyond the polar regions, the extent and duration of global and regional snow cover affect climate on numerous scales. The effects of snow cover on temperature have been identified in both empirical analyses and modeling efforts. The higher surface albedo when snow is present is responsible for reducing air temperatures in the lower troposphere (e.g., Dewey 1977; Baker et al. 1992; Walsh et al. 1982). This effect is largest during Northern Hemisphere spring when snow cover is most extensive and solar illumination is high (Groisman et al. 1994). Ellis and Leathers (1998) have shown that, through the albedo effect, snow cover over the Great Plains depresses airmass temperatures by 1°–4°C. Remote effects of snow albedo on regional climate have been identified by Clark (1998) where he showed that snow extent anomalies over East Asia initiate a chain of atmospheric patterns that, downstream, are manifested in significant circulation changes over western North America.

Studies using multispectral satellite data, such as AVHRR, have had some success in computing surface albedo (Stroeve et al. 1997; Haefliger et al. 1993; De Abreu et al. 1994; Knap and Oerlemans 1996; Lindsay and Rothrock 1994). However, the accuracy does not meet the requirement for climate studies. For example, Barry (1985) recommends an uncertainty of 0.02 in the surface albedo. In the work by Stroeve et al. (1997), the satellite-derived albedo was accurate to

within 5% for dry snow and much more uncertain for melting snow. The difficulty in computing the surface albedo from satellite radiances is partly a result of the intervening atmosphere. Stroeve et al. (1997) showed that the atmospheric correction is most sensitive to aerosol amounts, with uncertainties of 50% in aerosol optical depth resulting in errors as large as 0.03 in surface albedo.

The anisotropic nature of snow reflectance must also be taken into account when retrieving surface albedos. Snow is a multiple scattering particulate medium comprising ice particles in a matrix of air. At visible wavelengths, ice particles are strongly forward scattering and transmit nearly all light. In the NIR, ice is moderately to strongly absorbing and larger grain sizes decrease reflectance. Forward scattering for a single ice particle increases slightly with wavelength. However, the forward scattering peak is enhanced more by the reduction in the number of scattering events than by the slight change in the phase function for ice (Warren 1982). When light absorbing particulates (dust or soot) are present, snow reflectance becomes more isotropic (Warren and Wiscombe 1980). Failure to accurately account for the bidirectional reflectance of snow, particularly at large viewing zenith angles, can lead to errors as large as 50% in the total outgoing flux (Steffen 1987). A 10% uncertainty in the conversion from bidirectional reflectance factor to albedo, for example, as a result of incorrect choice of grain size in the snow model, can lead to albedo errors as large as 0.06 (Stroeve et al. 1997).

Multiangle observations provide a unique opportunity to improve the accuracy of the satellite-derived surface albedo over snow- and ice-covered surfaces in two significant ways. First, they enable the use of physical models of snow BRDF, leading to additional improvements in the estimation of albedo. As with the case of clouds, described above in section 2a, supplementing multiangle data with physical scene models can lead to significant improvements in albedo accuracy, in this case by helping to identify the snow type and thus the appropriate angular model (e.g., for new, old, or wet snow). Second, as discussed above in section 2b, such data provide improved estimates of aerosol optical depth and particle type, enabling more accurate atmospheric corrections.

Snow angular measurements and models are currently limited over snow- and ice-covered surfaces. Some in situ spectral bidirectional reflectance measurements have been made by Steffen (1987, 1996) and Nolin et al. (1994) in Greenland, and Winthur (1994) and Warren et al. (1998) in Antarctica. Middleton and Mungall (1952), Dirmhirn and Eaton (1975), and Dozier et al. (1988) have measured angular reflectance over seasonal snowpacks. Knap and Reijmer (1998) have also made some limited snow bidirectional reflectance measurements over melting glacier ice. Top-of-atmosphere (TOA) angular models are also available (Taylor and Stowe 1984; Lindsay and Rothrock 1994); however, it is known that there are problems with these models (Dlhopolsky and Cess 1993), particularly over snow/ice surfaces (Li 1996).

These problems are directly addressable by combining simultaneous multiangle observations, corrected for atmospheric effects, with physically based models of snow multiangle reflectance. As described earlier, the optical properties of ice are well known and snow can be treated as a multiple scattering case. The optical properties of the snow, calculated from Mie theory, can be used as input to the Discrete Ordinate Radiative Transfer (DISORT) model (Stamnes et al. 1988), which calculates both the directional reflectance as well as the albedo. This approach allows the model to be used for a wide range of illumination conditions, solar and viewing geometries, and snowpack physical properties. The advantage of a multiangle sensor is that it provides a sampling of points at which bidirectional reflectance is measured, thus enabling the angular distribution of reflected radiation and the albedo to be reconstructed by fitting the multiangle data to the DISORT model results. This approach has been tested in ice sheet (Nolin et al. 1994; Nolin and Stroeve 1997; Stroeve et al. 1997) and montane applications (Nolin 1995) and, though not fully validated, has been shown to be highly successful under many conditions. One area where it will need further improvement is in the case of snow cover with a rough surface (such as the South Pole region of Antarctica). In this case, a semiempirical approach incorporating the approximate dimensions and orientations of sastrugi (small-scale wind erosion features on the snow surface) would be warranted (Warren et al. 1998). Multiangle measurements, being sensitive to geometric structure of the reflecting surface, should be able to provide additional information needed to characterize the surface and better determine albedo.

We present two examples illustrating the need to accurately account for snow BRDF. These examples use single-view-angle images but the approach would be similar for multiangle observations. Figure 5 shows the surface albedo averaged for August 1989 as de-

rived from AVHRR for the Greenland ice sheet (a) assuming that the surface is Lambertian, (b) retrieved from apparent surface reflectance using the DISORT model BRDF conversion technique, and (c) the difference between (a) and (b). Differences are seen not only in the magnitude of the surface albedo, but also the spatial distribution of areas of high and low albedo. The case incorporating BRDF more accurately represents the spatial distribution of albedo found over the ice sheet, showing that the surface albedo remains high and relatively constant for the high elevation regions (~0.82), and decreases substantially along the western and eastern coasts (10%–20% decrease). Large drops are also observed along the southern tip and the northeast parts of the ice sheet (10%–15% decrease). Maximum albedo values are found on South Dome in southern Greenland and a small area on the middle-west slope extending from approximately 69.5°N at an elevation of 2700 m above sea level (ASL) to the area north of Melville Bay (71°N) at approximately 1500 m ASL. During summer, this region receives substantial amounts of precipitation from upslope advection from the west (Ohmura and Reeh 1991). Low values of albedo are found in northeastern Greenland and are consistent with this region being the lowest precipitation area of the ice sheet (Ohmura and Reeh 1991; Bromwich and Robasky 1993). A second example of the importance of converting apparent surface reflectance to surface albedo can be seen in Fig. 6. Image data were acquired over Mammoth Mountain, California, using the Airborne Visible/Infrared Imaging Spectrometer (AVIRIS), a 224-channel instrument with 20-m spatial resolution. The image on the top is centered over the crest of the mountain. This NIR (1.03 μm) image has been atmospherically corrected to obtain apparent surface reflectance and has values ranging from 0.0 to 1.6. After application of the BRDF conversion technique using DISORT and a digital elevation model, snow albedo values on both sides of the crest range from 0.70 to 0.85. The resulting values, displayed in the bottom image, closely correspond to measured values from a surface meteorological station. Such conversions are essential if snowmelt models are to incorporate remotely sensed albedo data for water resources applications. Here we have demonstrated the

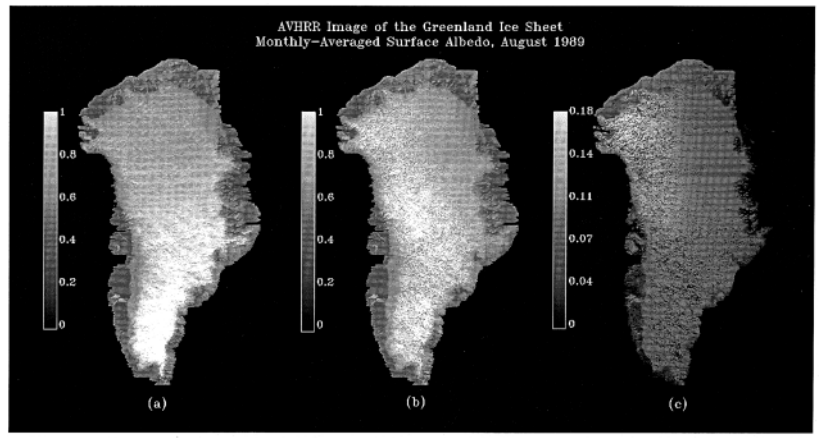

FIG. 5. Monthly averaged surface albedo during Aug 1989 over the Greenland ice sheet as derived from AVHRR visible and near-infrared radiances. (a) The surface albedo derived assuming the snow surface is Lambertian, (b) the surface albedo using the DISORT BRDF conversion technique, and (c) the difference between (a) and (b).

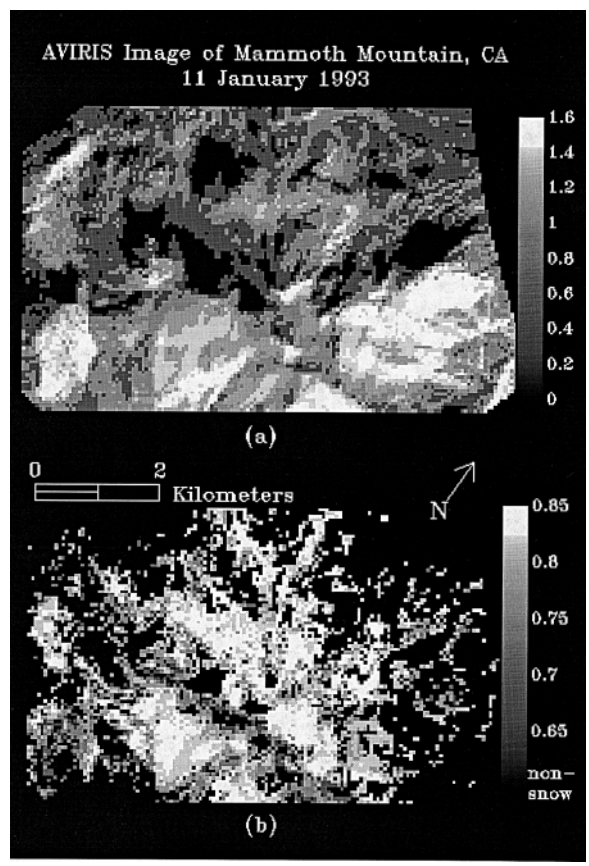

FIG. 6. Surface spectral albedo for Mammoth Mountain, CA, as derived from an atmospherically corrected subset of an AVIRIS image. (a) Apparent surface reflectance and (b) the surface albedo after application of the DISORT BRDF conversion algorithm and a USGS 7.5′ digital elevation model. The mountain was mostly snow covered at the time of the overpass (1030 local time, 11 Jan 1993). Non-snow-covered pixels and completely shadowed areas have been masked to black in (b).

advantages of single-angle corrections using model BRDFs. Simultaneous multiangle observations of snow covered surfaces would enable retrieval of albedo directly, leading to further improvement in accuracy.

d. Land vegetation–atmosphere interactions

How does land vegetation affect the partitioning of energy and mass between the surface and atmosphere? Beyond its application to snow and ice covers, albedo remains one of the most important parameters governing surface radiation budget (Dickinson 1983; Sellers et al. 1995). Charney (1975) first pointed out that changes in land cover, particularly associated with a reduction in vegetative cover fraction resulting from desertification in semiarid areas due to overgrazing practices, could lead to increased albedo which would enhance a so-called biophysical feedback mechanism and subsequently lead to reductions in rainfall. Although the proposed mechanism is no longer accepted as being so simple, a number of authors have investigated how drastic changes in land cover type and/or vegetative fraction due to deforestation can lead to enhanced albedo (Bastable et al. 1993; Dickinson and Henderson-Sellers 1988; Lean and Rowntree 1993) and subsequent reduced rainfall, and how increases in desertification could also lead to the same consequences (Sud and Fennessy 1982). Henderson-Sellers and Wilson (1983) argue that general circulation models (GCMs) require surface albedo with an uncertainty of 0.01–0.05 and a maximum sampling time of 1 month. Graetz (1991) also showed why high accuracy is required for albedo retrievals to predict large-scale climate patterns correctly; Lean and Rowntree (1993) showed that a change in albedo of 5% could lead to decreases in rainfall of 5% with large impacts in tropical forested areas. The Project for Intercomparison of Land-Surface Parameterization Schemes (PILPS) is a major community effort currently under way to enhance the land surface process models that drive the boundary layer radiative and convective processes in both climate and weather prediction models (Henderson-Sellers et al. 1993, 1995; Shao and Henderson-Sellers 1996; Qu et al. 1998). Multiangle measurements are crucial to providing the accurate specification of surface anisotropy and albedo needed for these efforts.

Spatial and temporal variability in biosphere–atmosphere CO_2 exchange is also a major global change research focus because of its link to climate and other earth system processes (IPCC 1995b). This issue has also received intense political attention following the meeting of the United Nations Environment Program in Kyoto, Japan, where protocols for the regulation of CO_2 emissions were discussed (IGBP 1998). Although the importance of the CO_2 issue is broadly agreed upon, efforts to evaluate linkages between human activities (e.g., land-use change, fossil fuel emissions), climate, and the carbon (C) cycle are only in the early stages of development. Important details about C cycle dynamics are still needed to understand basic earth system function (Schimel 1995), upon which an understanding of human impacts can be built. However, these details remain elusive because no one measurement program can address the temporal and spatial complexity of the biogeochemical and atmospheric processes involved in regulating the C cycle.

Remote sensing is gaining a major role in filling the gap between local-to-landscape level efforts and global-scale atmospheric research programs by providing spatially and temporally contiguous measurements of key components of the C cycle (Wessman and Asner 1998). Only in the last five years have data with the requisite spatial and temporal characteristics become widely available (e.g., James 1994). Currently, AVHRR provides the only decadal or longer time series of global terrestrial radiance measurements needed to evaluate certain key components of the C cycle. AVHRR provides the most common metric used to evaluate vegetation dynamics—the Normalized Difference Vegetation Index (NDVI)—which is the difference between NIR and red surface reflectances divided by their sum. While the NDVI is simply a radiometric quantity, there is a theoretical and empirical basis for a link between it and certain vegetation properties (Asrar et al. 1984; Sellers 1987). The link is made through relationships between NDVI and the fraction of photosynthetically active radiation absorbed by plant canopies (fAPAR), which is largely determined by the amount, spatial orientation, and condition of green foliage present (Myneni and Williams 1994) and, in turn, to net primary productivity (NPP), which is a critical component of the C cycle because it represents the net amount of C assimilated by plants through time. NPP has a major impact on subsequent processes of decomposition, respiration, and ultimately carbon storage (Randerson et al. 1997). Through the use of light-use efficiency factors that convert energy units to carbon uptake values (Field et al. 1995), NDVI has been used to estimate NPP on a seasonal and interannual basis. However, while the NDVI effort has provided some useful insight to the

dynamics of the terrestrial C cycle, its utility and success have been sharply limited by factors that impede the interpretation and employment of these data.

First, major sources of error exist in the current NDVI approach, limiting its quantitative capability to resolve persisting uncertainties in the spatial and temporal dynamics of terrestrial C uptake (Asner et al. 1998b). Changes in solar zenith angle from AVHRR drift and the earth's seasonal cycle sharply impact the NDVI (Meyer et al. 1995; Privette et al. 1995). Moreover, all global, high temporal resolution remote sensing instruments employ off-nadir observations (via wide swath) to achieve worldwide coverage, and thus the viewing geometry of the measurements varies in space and time (Barnsley et al. 1994). These geometric factors would not matter if land surface (e.g., vegetation, soils) and atmospheric (e.g., clouds, aerosols) constituents were isotropic reflectors. However, their macro- and microphysical construction does lead to significant directional reflectance variability with changing illumination and viewing geometry (see Fig. 2), and other factors controlling the shape of the BRDF of the land surface include vegetation clumping (Li et al. 1995), self-shadowing within canopies due to foliage orientation and other architectural attributes (Goel 1988), and soil roughness (Jacquemoud et al. 1992).

Second, and perhaps more fundamentally, the NDVI-based approach cannot solve the CO_2 exchange problem without the use of a preassigned land cover map; however, inaccuracies in such a map, or changes in land cover not represented by a static map, can lead to misinterpretation of remotely sensed data. An example of this is demonstrated in Fig. 7. Any pixel can be depicted as a point on the red-NIR plane. For each biome type a data density distribution function defined as number of pixels per unit red-NIR plane was evaluated using LASUR (Land Surface Reflectances) derived from AVHRR data. Each biome-dependent contour in Fig. 7 separates an area of the highest data density and contains 25% of pixels from a given biome type. These areas can be interpreted as the sets of pixels representing the most probable patterns of canopy structure. Pixels having the same value of NDVI lie on a single line in the red-NIR spectral space. One can see that the canopy structure can vary considerably with NDVI unchanged. Thus, even a high degree of accuracy in the NDVI cannot improve its information content.

The role of multiangle measurements in improving ecological and biogeochemical research falls into three major categories: retrieval of ground cover BRDF, and hence albedo; capitalizing on the biogeophysical information represented by the anisotropic reflectance characteristics of vegetation and soils; and accounting for atmospheric properties that affect the accuracy of the derived surface reflectance data, as discussed in section 2b. These issues have been raised in previous work (e.g., Li et al. 1995; Verstraete et al. 1996; Myneni et al. 1997; Knyazikhin et al. 1998b; Pinty et al. 1998b). Several of these studies show that multiangle measurements provide access to surface parameters by mining their anisotropic reflectance characteristics rather than relegating this information to the status of noise requiring suppression or removal. For example, when the vegetation–soil BRDF is analyzed quantitatively, it is possible to estimate leaf area index (LAI) and fAPAR while accounting for the vegetation structural characteristics that impact the angular reflectance values (e.g., Goel and Strebel 1983; Camillo 1987; Privette et al. 1996, 1997b; Gobron et al. 1997a; Knyazikhin et al. 1998a). Single-angle vegetation index measurements cannot resolve spatial and temporal changes in plant structural characteristics, such as leaf angle distributions, canopy clumping, and landscape heterogeneity. Yet these factors largely determine the angular reflectance distribution of vegetated landscapes, and therefore complicate efforts to estimate variables such as LAI and fAPAR (Myneni

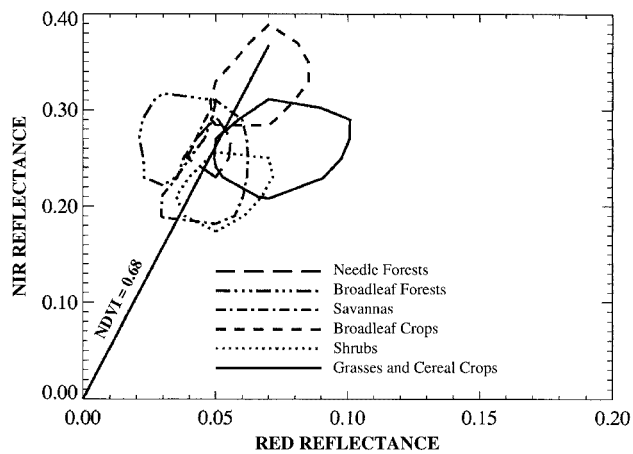

FIG. 7. Distribution of vegetated pixels from LASUR data with respect to their reflectances at red and NIR wavelengths. Each biome-dependent contour separates a set of pixels representing most probable patterns of canopy structure from a given biome type. Pixels having the same value of NDVI lie on a single line in the red-NIR spectral space. One can see that canopy structure can vary considerably with NDVI unchanged. Prototyping of the MISR LAI and fAPAR retrievals using POLDER data show that the use of multiangle data can help to identify the biome type (Zhang et al. 1999, unpublished manuscript).

and Williams 1994). In other words, there is too little information in a single-angle reflectance metric to fully resolve the suite of vegetation properties that create variation in that metric. Multiangle data provide access to entirely new vegetation structural variables that directly impact estimates of fAPAR, LAI, and NPP, and could play an additional role in measuring and monitoring key aspects of the C cycle (Asner et al. 1998b).

The following examples indicate that the use of multiangle data improves the accuracy and reliability of retrieved biophysical parameters. The first example is for shrubs, a biome type that exhibits lateral spatial heterogeneity, low to intermediate vegetation ground cover, and bright background. We retrieved two LAI fields from POLDER data using the MISR LAI–fAPAR retrieval technique (Knyazikhin et al. 1998a). POLDER surface reflectances at one (near-nadir) and six view directions, respectively, were used to derive these fields. Then, NDVI–LAI regression curves were estimated using the retrieved LAI fields and POLDER data. These regression curves are shown in Fig. 8 (top). The MISR LAI–fAPAR algorithm performs the retrievals by comparing observed and modeled radiances for a suite of canopy structure and soil patterns that covers a range of expected natural conditions. The set of all canopy/soil patterns for which the magnitude of the residuals in the comparison does not exceed uncertainties in observed radiances are treated as acceptable solutions. The mean over all acceptable LAI values and its dispersion (standard deviation) are taken as a retrieved LAI value and the accuracy in LAI retrievals, respectively. The accuracy (dispersion) in the retrieved LAI fields is shown in Fig. 8 (bottom). For a nadir-viewing instrument whose footprint does not spatially resolve individual scene elements, the information conveyed about the canopy structure is small and a wide range of natural variation in ground cover and soil can result in the same value of the remotely sensed signal (see curve labeled "1 view angle" in the bottom part of Fig. 8). However, since the interaction of photons with the canopy structure governs the off-nadir directional reflectance distribution, inclusion of additional angular information tends to improve the accuracy in the retrieved canopy structural parameters (see curve labeled "6 view angles"). Another extreme situation is the case of a dense canopy, in which its reflectance in one or several directions can be insensitive to the various parameter values characterizing the canopy. When this happens, the canopy reflectance is said to belong to the saturation domain. Therefore, the reliability of parameters retrieved under a condition of saturation is very low (Gobron et al. 1997b). Figure 9 demonstrates the accuracy in LAI values retrieved under a condition of saturation as a function of number of view directions. POLDER vegetated land surface pixels whose reflectances at a single near-nadir direction belonged to the saturation domain were selected to retrieve two LAI fields using the same single-angle near-nadir direction and six view directions, respectively. Reflectances of broadleaf crops, savannas, and broadleaf forests mainly constituted the saturation domain. The use of multiangle information results in fewer solutions that were deemed consistent with the observations and the retrieval uncertainty in LAI is consequently reduced.

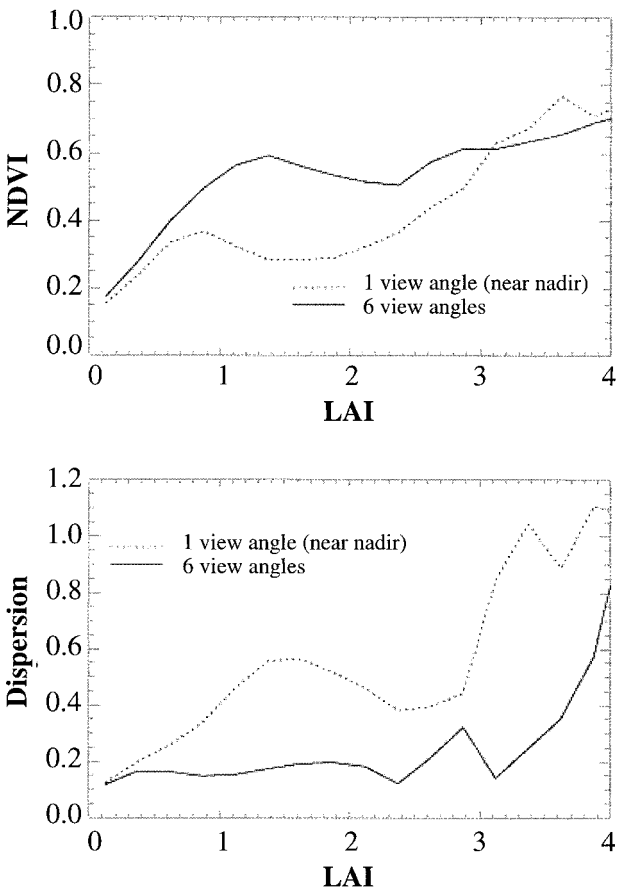

FIG. 8. NDVI–LAI regression curves for shrubs (top) and the accuracy in shrubs–LAI retrievals (bottom) derived from POLDER data using single (points) and simultaneous multiangle (line) observations. The horizontal and vertical axes of the bottom figure show the retrieved LAI and its dispersion, respectively. The use of multiangle information tends to improve the accuracy in the LAI retrievals and, as a consequence, the form of the NDVI–LAI relationship.

In recent work, multiangle measurements were used with a three-dimensional canopy radiative transfer model to characterize vegetation structure of a savanna region in the southwest United States (Asner et al. 1997, 1998a). In this particular application, the radiative transfer model provided the physical basis in which canopy structural variables, such as leaf angle distribution, could be constrained while parameters of interest (LAI and vegetation cover) were estimated using inverse modeling techniques. Numerical inversion of this "constrained model" with multiangle reflectance data allowed for LAI and vegetation cover estimates that could be directly related to variation in land cover and land use. Carbon cycle modeling with the retrieved structural information showed that canopy and landscape structure played a major role in determining CO_2 fluxes in spatially heterogeneous environments. A comparison with the NDVI-based approach indicated that the multiangle method was more accurate in estimating LAI because it explicitly accounted for structural heterogeneity and canopy shading. Analogous approaches that integrate multiangle observations with radiative transfer models to identify the biome type have been developed for operational use on the EOS Terra mission (Knyazikhin et al. 1998a,b). Errors in fAPAR and NPP are estimated to decrease from approximately 20%–40% currently to 2%–10% in the EOS era (Running et al. 1994), a conclusion supported by sensitivity studies indicating that such accuracy improvements are achieved with about seven view angles over the hemisphere (Lucht 1998).

Beyond this type of approach for estimating LAI and NPP in structurally complex ecosystems, multiangle measurements can provide estimates of the gap fraction between individual trees in forested regions (Barker-Schaaf and Strahler 1994; Li et al. 1995; Gerard and North 1997). Forest canopy gap fraction is an important parameter in many ecosystem and land surface models (e.g., Lindner et al. 1997). Through an integration of these improved remote sensing capabilities, atmospheric CO_2 monitoring, and modeling, a better understanding of the temporal and spatial variability of terrestrial C sources and sinks will be achieved, leading to more reliable prognostic analyses of human impacts on climate and other earth system processes.

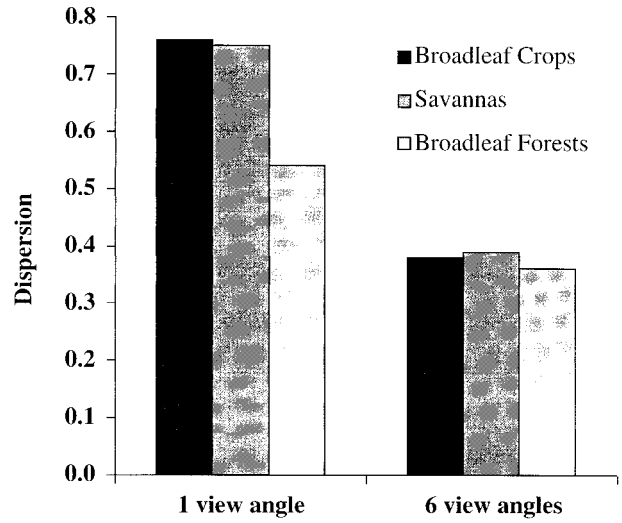

FIG. 9. The accuracy in LAI values retrieved under a condition of saturation as a function of number of view directions of broadleaf crops, savannas, and broadleaf forests. POLDER surface reflectances at one (near-nadir) and six view directions were used. The lower dispersion of retrieved LAI values shows that the availability of simultaneous multiangle observations improves the reliability of the LAI retrievals.

3. Conclusions

This paper illustrates the benefits of simultaneous multiangle observing as applied to a set of questions in various scientific disciplines. Simultaneous multiangle sampling enables both a decrease in the level of noise on retrieved geophysical parameter values, and at the same time, an increase in their reliability, for several reasons. First, it does not require the use of temporal aggregations as a proxy for multiangle sampling, thus avoiding potentially incorrect assumptions about the stability of the geophysical system and the attendant risk of increasing noise rather than isolating the sought-after signal. Second, multiangle observation facilitates the implementation of advanced algorithms that are designed to separate out the various contributors to the remotely sensed signal, for example, surface radiative properties and atmospheric effects. Finally, the inclusion of the angular domain (in addition to spectral sampling) is a prerequisite to constraining the inversion process and limiting the number of acceptable solutions. By providing additional information that constrains the physical nature of the scene being observed, whether it be an identification of aerosol type, cloud height and form, or surface cover, there is an attendant increase in confidence in the uniqueness of the retrieved signal and considerably reduced ambiguity and error in the retrieved geophysical or biophysical parameters.

The nature of the physical problem of radiation transfer through complex geophysical interfaces and

inside mostly heterogeneous media, and the level of product sophistication and accuracies that are required in a number of scientific applications, are such that retrieval algorithms must establish real-time physical scene information rather than employing statistically based or empirical models or predetermined, static scene maps. Multiangle data acquisition systems provide a means for addressing this situation and enabling extraction of high-level and accurate geophysical products. We argue for their continued inclusion as part of future remote sensing missions.

Acknowledgments. D. Diner's research is performed at the Jet Propulsion Laboratory, California Institute of Technology, under contract with the National Aeronautics and Space Administration (NASA). G. Asner is supported by the NASA Interdisciplinary Science Program, NASA Land-cover/Land-use Change Program, and the Mellon Foundation. R. Davies is supported by Contract 960489 from the Jet Propulsion Laboratory, California Institute of Technology. Y. Knyazikhin's research is performed at the Department of Geography, Boston University, under contract with NASA. J.-P. Muller is supported by NERC and by the European Commission under the Fourth Framework research program. A. Nolin and J. Stroeve are supported by NASA Grant NAG5-6462. B. Pinty thanks his collaborators for fruitful discussions and acknowledges the support of the Space Applications Institute of the European Commission. C. Schaaf is supported by NASA under NAS5-31369 as part of the MODIS program. This paper is an outgrowth of discussions held during the International Forum on BRDF in San Francisco, California, on 11–12 December 1998, and we thank the participants of those discussions. We also thank R. Kahn and J. Martonchik for helpful comments on the manuscript.

References

Ackerman, S. A., K. I. Strabala, W. P. Menzel, R. A. Frey, C. C. Moeller, and L. E. Gumley, 1998: Discriminating clear sky from clouds with MODIS. *J. Geophys. Res.*, **103,** 32 141–32 157.

Arking, A., 1991: The radiative effects of clouds and their impact on climate. *Bull. Amer. Meteor. Soc.*, **72,** 795–813.

——, C. A. Wessman, and J. L. Privette, 1997: Unmixing the directional reflectance of AVHRR sub-pixel landcovers. *IEEE Trans. Geosci. Remote Sens.*, **35,** 868–881.

——, B. H. Braswell, D. S. Schimel, and C. A. Wessman, 1998a: Ecological research needs from multi-angle remote sensing data. *Remote Sens. Environ.*, **63,** 155–165.

——, C. A. Bateson, J. L. Privette, N. El Saleous, and C. A. Wessman, 1998b: Estimating vegetation structural effects on carbon uptake using satellite data fusion and inverse modeling. *J. Geophys. Res.*, **103,** 28 839–28 853.

Asrar, G., M. Fuchs, E. T. Kanemasu, and M. Yoshida, 1984: Estimating absorbed photosynthetically active radiation and leaf area index from spectral reflectance in wheat. *Agron. J.*, **76,** 300–306.

Baker, D. G., D. L. Ruschy, R. H. Skaggs, and D. B. Wall, 1992: Air temperature and radiation depressions associated with a snowcover. *J. Appl. Meteor.*, **31,** 247–254.

Barker-Schaaf, C., and A. H. Strahler, 1994: Validation of bidirectional and hemispherical reflectances from a geometric-optical model using ASAS imagery and pyranometer measurements of a spruce forest. *Remote Sens. Environ.*, **49,** 138–151.

Barnsley, M. J., A. H. Strahler, K. P. Morris, and J.-P. Muller, 1994: Sampling the surface bidirectional reflectance distribution function: 1. Evaluation of current and future satellite sensors. *Remote Sens. Rev.*, **8,** 271–311.

Barry, R. G., 1985: The cryosphere and climate change. *Detecting the Climate Effects of Increasing CO_2*. M. C. MacCracken and F. M. Luther, Eds., U.S. Department of Energy, 109–141.

Bastable, H. G., W. J. Shuttleworth, R. L. G. Dallarosa, G. Fisch, and C. A. Nobre, 1993: Observations of climate, albedo and surface radiation over cleared and undisturbed Amazonian forest. *Int. J. Climatol.*, **13,** 783–796.

Baum, B. A., and Coauthors, 1995: Imager clear-sky determination and cloud detection (Subsystem 4.1), Clouds and the Earth's Radiant Energy System (CERES) Algorithm Theoretical Basis Document, Volume III: Cloud Analyses and Radiance Inversions (Subsystem 4). *NASA RP 1376*, **3,** 43–82.

Bintanja, R., and M. R. Van den Broeke, 1996: The influence of clouds on the radiation budget of ice and snow surfaces in Antarctica and Greenland in summer. *Int. J. Climatol.*, **16,** 1281–1296.

Bromwwich, D. H., and F. M. Robasky, 1993: Recent precipitation trends over the polar ice sheets. *Meteor. Atmos. Phys.*, **51,** 259–274.

Cabot, F., and G. Dedieu, 1997: Surface albedo from space: Coupling bidirectional models and remotely sensed measurements. *J. Geophys. Res.*, **102,** 19 645–19 663.

Camillo, P., 1987: A canopy reflectance model based on an analytical solution to the multiple scattering equation. *Remote Sens. Environ.*, **23,** 453–477.

Charlock, T. P., and V. Ramanathan, 1985: The albedo field and cloud radiative forcing produced by a general circulation model with internally generated cloud optics. *J. Atmos. Sci.*, **42,** 1408–1429.

Charlson, R. J., J. Langner, H. Rodhe, C. B. Leovy, and S. G. Warren, 1991: Perturbation of the northern hemispheric radiative balance by backscattering from anthropogenic sulfate aerosols. *Tellus*, **43AB,** 152–163.

——, S. Schwartz, J. Hales, R. Cess, J. Coakley Jr., J. Hansen, and D. Hoffmann, 1992: Climate forcing by anthropogenic aerosols. *Science*, **255,** 423–430.

Charney, J. G., 1975: Dynamics of deserts and drought in the Sahel. *Quart. J. Roy. Meteor. Soc.*, **101,** 193–202.

Clark, M. P., 1998: The role of snow cover in the climate system. Ph.D. dissertation, Dept. of Geology, University of Colorado, 108 pp.

Davies, R., and T. Várnai, 1997: Albedo algorithms and errors from multiangle satellite measurements. *IRS'96 Current Problems in Atmospheric Radiation*, W. L. Smith and K. Stamnes, Eds., 770–773.

De Abreu, R. D., D. G. Barber, K. Misurak, and E. F. Le Drew, 1994: Spectral albedo of snow-covered first-year and multiyear sea ice during spring melt. *Ann. Glaciol.*, **21,** 288–297.

d'Entremont, R. E., C. L. Barker Schaaf, W. Lucht, and A. H.

Strahler, 1999: Retrieval of red spectral albedo and bidirectional reflectance using AVHRR HRPT and GOES satellite observations of the New England region. *J. Geophys. Res.*, **104,** 6229–6239.

Deschamps, P.-Y., F-M. Bréon, M. Leroy, A. Podaire, A. Bricaud, J.-C. Buriez, and G. Sèze, 1994: The POLDER mission: Instrument characteristics and scientific objectives. *IEEE Trans. Geosci. Remote Sens.*, **32,** 598–615.

Dewey, K. F., 1977: Daily maximum and minimum temperature forecasts and the influence of snow cover. *Mon. Wea. Rev.*, **105,** 1594–1597.

Dickinson, R. E., 1983: Land surface processes and climate—Surface albedos and energy balance. *Advances in Geophysics,* Vol. 25, Academic Press, 305–353.

——, and A. Henderson-Sellers, 1988: Modeling tropical deforestation: A study of GCM land–surface parameterizations. *Quart. J. Roy. Meteor. Soc.*, **114,** 439–462.

Di Girolamo, L. and R. Davies, 1994: A band-differenced angular signature technique for cirrus cloud detection. *IEEE Trans. Geosci. Remote Sens.*, **32,** 890–896.

Diner, D. J., and Coauthors, 1997a: MISR level 2 cloud detection and classification algorithm theoretical basis. JPL Internal Doc. D-11399, 98 pp. [Available from JPL Documentation Services, 4800 Oak Grove Dr., Pasadena, CA 91109.]

——, L. Di Girolamo, and E. E. Clothiaux, 1997b: MISR level 1 cloud detection algorithm theoretical basis. JPL Internal Doc. D-13397, 37 pp. [Available from JPL Documentation Services, 4800 Oak Grove Dr., Pasadena, CA 91109.]

——, and Coauthors, 1998a: The Airborne Multi-angle Imaging SpectroRadiometer (AirMISR): Instrument description and first results. *IEEE Trans. Geosci. Remote Sens.*, **36,** 1339–1349.

——, and Coauthors: 1998b: Multi-angle Imaging SpectroRadiometer (MISR) instrument description and experiment overview. *IEEE Trans. Geosci. Remote Sens.*, **36,** 1072–1087.

Dirmhirn, I., and F. D. Eaton, 1975: Some characteristics of the albedo of snow. *J. Appl. Meteor.*, **14,** 375–379.

Dlhopolsky, R., and R. D. Cess, 1993: Improved angular directional models for clear sky ocean derived from Earth Radiation Budget Satellite shortwave radiances. *J. Geophys. Res.*, **98,** 16 713–16 721.

Dozier, J., R. E. Davis, A. T. C. Chang, and K. Brown, 1988: The spectral bidirectional reflectance of snow. *Proc. 4th Int. Colloq. on Spectral Signatures of Objects in Remote Sensing*, Aussois, France, European Space Agency, 87–92.

Ellis, A. W., and D. J. Leathers, 1998: The effects of a discontinuous snow cover on lower atmospheric temperature and energy flux patterns. *Geophys. Res. Lett.*, **25,** 2161–2164.

Field, C. B., J. T. Randerson, and C. M. Malmstrom, 1995: Global net primary production: Combining ecology and remote sensing. *Remote Sens. Environ.*, **51,** 74–88.

Gerard, F. F., and P. R. J. North, 1997: Analyzing the effect of structural variability and canopy gaps on forest BRDF using a geometric–optical model. *Remote Sens. Environ.*, **62,** 46–61.

Gesell, G., 1989: An algorithm of snow and ice detection using AVHRR data: An extension to the APOLLO software package. *Int. J. Remote Sens.*, **10,** 897–905.

Gobron, N., B. Pinty, M. M. Verstraete, and Y. Govaerts, 1997a: Presentation and application of an advanced model for the scattering of light by vegetation in the solar domain. *Physical Measurements and Signatures in Remote Sensing*, G. Guyot and T. Phulpin, Eds., ISPRS, 267–273.

——, ——, and ——, 1997b: Theoretical limits to the estimation of the leaf area index on the basis of optical remote sensing data. *IEEE Trans. Geosci. Remote Sens.* **35,** 1438–1445.

Goel, N. S., 1988: Models of vegetation canopy reflectance and their use in estimation of biophysical parameters from reflectance data. *Remote Sens. Rev.*, **4,** 1–212.

——, and D. E. Strebel, 1983: Inversion of vegetation canopy reflectance models for estimating agronomic variables. I. Problem definition and initial results using Suits model. *Remote Sens. Environ.*, **13,** 487–507.

Graetz, R. D., 1991: The nature and significance of the feedback of changes in terrestrial vegetation on global atmospheric and climatic-change. *Climate Change*, **18,** 147–173.

Groisman, P. Ya., T. R. Karl, and R. W. Knight, 1994: Observed impact of snow cover on the heat balance and the rise of continental spring temperatures. *Science*, **263,** 198–200.

Gustafson, G., and Coauthors: 1994: Support of Environmental Requirements for Cloud Analysis and Archive (SERCAA): Algorithm descriptions. Rep. PL-TR-94-2114, Phillips Laboratory, 100 pp. [Available from Hanscom AFB, MA 01731.]

Haefliger, M., K. Steffen, and C. Fowler, 1993: AVHRR surface temperature and narrow-band albedo comparison with ground measurements for the Greenland ice sheet. *Ann. Glaciol.*, **17,** 49–54.

Hasler, A. F., 1981: Stereographic observations from satellites: An important new tool for the atmospheric sciences. *Bull. Amer. Meteor. Soc.*, **62,** 194–212.

Hautecoeur, O., and M. M. Leroy, 1998: Surface bidirectional reflectance distribution function observed at global scale by POLDER/ADEOS. *Geophys. Res. Lett.*, **25,** 4197–4200.

Henderson-Sellers, A., and M. F. Wilson, 1983: Surface albedo data for climate modelling. *Rev. Geophys. Space Phys.*, **21,** 1743–1778.

——, Z.-L. Yang, and R. E. Dickinson, 1993: The Project for Intercomparison of Land-Surface Parameterization Schemes (PILPS). *Bull. Amer. Meteor. Soc.*, **74,** 1335–1349.

——, A. Pitman, P. Love, P. Irannejad, and T. Chen, 1995: Project for Intercomparison of Land-Surface Parameterization Schemes (PILPS): Phases 2 and 3. *Bull. Amer. Meteor. Soc.*, **76,** 489–503.

Hu, B., W. Lucht, and A. H. Strahler, 1999: The interrelationship of atmospheric correction of reflectances and surface BRDF retrieval: A sensitivity study. *IEEE Trans. Geosci. Remote Sens.*, **37,** 724–738.

Husar, R. B., J. M. Prospero, and L. L. Stowe, 1997: Characterization of tropospheric aerosols over the oceans with the NOAA Advanced Very High Resolution Radiometer optical thickness operational product. *J. Geophys. Res.*, **102,** 16 889–16 909.

IGBP Carbon Cycle Working Group, 1998: The terrestrial carbon cycle: Implications for the Kyoto Protocol. *Science*, **280,** 1393–1397.

IPCC, 1995a: *Climate Change 1995, Report of the Intergovernmental Panel on Climate Change.* Cambridge University Press, 64 pp.

——, 1995b: *Impacts, Adaptations, and Mitigation of Climatic Change–Technical Analyses.* Cambridge University Press, 878 pp.

Jacquemoud, S., F. Baret, and J. F. Hanocq, 1992: Modeling spectral and bidirectional soil reflectance. *Remote Sens. Environ.*, **41,** 123–132.

James, M. E., 1994: The Pathfinder AVHRR land data set. *Int. J. Remote Sens.*, **15,** 3315–3326.

Kahn, R., R. West, D. McDonald, B. Rheingans, and M. I. Mishchenko, 1997: Sensitivity of multi-angle remote sensing observations to aerosol sphericity. *J. Geophys. Res.*, **102,** 16 861–16 870.

——, P. Banerjee, D. McDonald, and D. J. Diner, 1998: Sensitivity of multiangle imaging to aerosol optical depth and pure-particle size distribution and composition over ocean. *J. Geophys. Res.*, **103,** 32 195–32 213.

Kiehl, J. T., and B. P. Briegleb, 1993: The relative roles of sulfate aerosols and greenhouse gases in climate forcing. *Science*, **260,** 311–314.

Kimes, D. S., P. J. Sellers, and D. J. Diner, 1987: Extraction of spectral hemispherical reflectance (albedo) of surfaces from nadir and directional reflectance data. *Int. J. Remote Sens.*, **8,** 1727–1746.

Knap, W. H., and J. Oerlemans, 1996: The surface albedo of the Greenland ice sheet: Satellite derived and in situ measurements in the Sondre Stromfjord area during the 1991 melt season. *J. Glaciol.*, **42,** 364–374.

——, and C. H. Reijmer, 1998: Anisotropy of the reflected radiation field over melting glacier ice: Measurements in Landsat TM bands 2 and 4. *Remote Sens. Environ.* **65,** 93–104.

Knyazikhin, Y., J. V. Martonchik, D. J. Diner, R. B. Myneni, M. M. Verstraete, B. Pinty, and N. Gobron, 1998a: Estimation of vegetation canopy leaf area index and fraction of absorbed photosynthetically active radiation from atmosphere-corrected MISR data. *J. Geophys. Res.*, **103,** 32 239–32 256.

——, ——, R. B. Myneni, D. J. Diner, and S. W. Running, 1998b: Synergistic algorithm for estimating vegetation canopy leaf area index and fraction of absorbed photosynthetically active radiation from MODIS and MISR data. *J. Geophys. Res.*, **103,** 32 257–32 275.

Koelemeijer, R. B. A., P. Stammes, and P. D. Watts, 1998: Comparison of visible calibrations of GOME and ATSR-2. *Remote Sens. Environ.*, **63,** 279–288.

Lean, J., and P. R. Rowntree, 1993: A GCM simulation of the impact of the Amazonia deforestation on climate using an improved canopy representation. *Quart. J. Roy. Meteor. Soc.*, **119,** 509–530.

Lee, T. Y., and Y. J. Kaufman, 1986: Non-Lambertian effect on remote sensing of surface reflectance and vegetation index. *IEEE Trans. Geosci. Remote Sens.*, **24,** 699–708.

Li, X., A. H. Strahler, and C. E. Woodcock, 1995: A hybrid geometric optical-radiative transfer approach for modeling albedo and directional reflectance of discontinuous canopies. *IEEE Trans. Geosci. Remote Sens.*, **33,** 466–480.

Li, Z., 1996: On the angular correction of satellite radiation measurements: The performance of ERBE angular dependence model in the Arctic. *Theor. Appl. Climatol.*, **54,** 235–248.

——, and H. G. Leighton, 1991: Scene identification and its effect on cloud radiative forcing in the Arctic. *J. Geophys. Res.*, **96,** 9175–9188.

——, J. Cilhar, X. Zhang, L. Moreau, and H. Ly, 1996: Detection and correction of the bidirectional effect in AVHRR measurements over northern regions. *IEEE Trans. Geosci. Remote Sens.*, **34,** 1308–1322.

Lindner, M., R. Sievaen, and H. Pretzsch, 1997: Improving the simulation of stand structure in a forest gap model. *Forest Ecol. Manage.*, **95,** 183–197.

Lindsay, R. W., and D. A. Rothrock, 1994: Arctic sea ice albedo from AVHRR. *J. Climate*, **7,** 1737–1749.

Lorenz, D., 1985: On the feasibility of cloud stereoscopy and wind determination with the Along-Track Scanning Radiometer. *Int. J. Remote Sens.*, **6,** 1445–1461.

Lucht, W., 1998: Expected retrieval accuracies of bidirectional reflectance and albedo from EOS-MODIS and MISR angular sampling. *J. Geophys. Res.*, **103,** 8763–8778.

——, C. Schaaf, and A. H. Strahler, 1999: An algorithm for the retrieval of albedo from space using semiempirical BRDF models. *IEEE Trans. Geosci. Remote Sens.*, in press.

Martonchik, J. V., and D. J. Diner, 1992: Retrieval of aerosol optical properties from multi-angle satellite imagery. *IEEE Trans. Geosci. Remote Sens.*, **30,** 223.

——, ——, R. A. Kahn, T. P. Ackerman, M. M. Verstraete, B. Pinty, and H. Gordon, 1998a: Techniques for the retrieval of aerosol properties over land and ocean using multiangle imaging. *IEEE Trans. Geosci. Remote Sens.*, **36,** 1212–1227.

——, D. J. Diner, B. Pinty, M. M. Verstraete, R. B. Myneni, Y. Knyazikhin, and H. R. Gordon, 1998b: Determination of land and ocean reflective, radiative, and biophysical properties using multiangle imaging. *IEEE Trans. Geosci. Remote Sens.*, **36,** 1266–1281.

Maykut, G. A., and N. Untersteiner, 1971: Some results from a time-dependent thermodynamic model of sea ice. *J. Geophys. Res.*, **76,** 1550–1575.

Meyer, D., M. M. Verstraete, and P. Pinty, 1995: The effect of surface anisotropy and viewing geometry on the estimation of NDVI from AVHRR. *Remote Sens. Rev.*, **12,** 3–27.

Middleton, W. E. K., and A. G. Mungall, 1952: The luminous directional reflectance of snow. *J. Opt. Soc. Amer.*, **42,** 572–579.

Mishchenko, M. I., A. A. Lacis, B. E. Carlson, and L. D. Travis, 1995: Nonsphericity of dust-like tropospheric aerosols: Implications for aerosol remote sensing and climate modeling. *Geophys. Res. Lett.*, **22,** 1077–1080.

Moroney, C., R. Davies, and R. Marchand, 1999: Cloud-top heights from AirMISR stereo measurements. Preprints, *10th Conf. on Atmospheric Radiation*, Madison, WI, Amer. Meteor. Soc., 110–113.

Myneni, R. B., and D. L. Williams, 1994: On the relationship between fAPAR and NDVI. *Remote Sens. Environ.*, **49,** 200–209.

——, R. R. Nemani, and S. W. Running, 1997: Estimation of global leaf area index and absorbed PAR using radiative transfer models. *IEEE Trans. Remote Sens.*, **35,** 1380–1395.

Nakamura, N., and A. H. Oort, 1988: Atmospheric heat budgets of the polar regions. *J. Geophys. Res.*, **93,** 9510–9524.

Nicodemus, F. E., J. C. Richmond, J. J. Hsia, I. W. Ginsberg, and T. Limperis, 1977: *Geometrical Considerations and Nomenclature for Reflectance, NBS Monogr.*, No. 160, National Bureau of Standards, U.S. Department of Commerce, 52 pp.

Nolin, A. W., 1995: Snow albedo from BRDF parameterizations. *Eos, Trans. Amer. Geophys. Union*, **76,** 185.

——, and J. Stroeve, 1997: The changing albedo of the Greenland Ice Sheet: Implications for climate change. *Ann. Glaciol.*, **25,** 51–57.

——, K. Steffen, and J. Dozier, 1994: Measuring and modeling the bidirectional reflectance of snow. *Proc. IGARSS'94 Symp.*, Pasadena, CA, IEEE, 1919–1921.

North, P. R. J., 1998: Dual-view operational atmospheric correction for ATSR-2 imagery. *Proc. IGARSS'98 Symp.*, Seattle, WA, IEEE. [Available on CD-ROM.]

Oerlemans, J., and N. C. Hoogendoorn, 1989: Mass-balance gradients and climatic change. *J. Glaciol.*, **35,** 399–405.

Ohmura, A., and N. Reeh, 1991: New precipitation and accumulation maps for Greenland. *J. Glaciol.*, **37,** 140–148.

Pinty, B., F. Roveda, M. M. Verstraete, N. Gobron, Y. Govaerts, G. Napoli, and J. Verdebout, 1998a: Meteosat surface albedo algorithm theoretical basis. EC Joint Research Centre Tech. Rep. EUR 18130 EN, 50 pp. [Available from JRC, TP440, Via E. Fermi, 1, I-21020 Ispra (VA), Italy.]

——, M. M. Verstraete, and N. Gobron, 1998b: The effect of soil anisotropy on the radiance field emerging from vegetation canopies. *Geophys. Res. Lett.*, **25,** 797–801.

Privette, J. L., C. Fowler, G. A. Wick, D. Baldwin, and W. J. Emery, 1995: Effects of orbital drift on Advanced Very High Resolution Radiometer products: Normalized difference vegetation index and sea surface temperature. *Remote Sens. Environ.*, **53,** 164–171.

——, W. J. Emery, and D. S. Schimel, 1996: Inversion of a vegetation reflectance model with NOAA AVHRR data. *Remote Sens. Environ.*, **58,** 187–200.

——, D. W. Deering, and D. E. Wickland, 1997a: Report on the Workshop on Multiangular Remote Sensing for Environmental Applications. NASA Tech. Memo. 113202, 56 pp. [Available from NASA Center for AeroSpace Information, Attn: STI Ordering Service, 7121 Standard Drive, Hanover, MD 21076-1320.]

——, T. F. Eck, and D. W. Deering, 1997b: Estimating spectral albedo and nadir reflectance through inversion of simple BRDF models with AVHRR/MODIS-like data. *J. Geophys. Res.*, **102,** 29 529–29 543.

Qu, W., and Coauthors, 1998: Sensitivity of latent heat flux from PILPS land-surface schemes to perturbations of surface air temperature. *J. Atmos. Sci.*, **55,** 1909–1927.

Ramanathan, V., R. D. Cess, E. F. Harrison, P. Minnis, B. R. Barkstrom, E. Ahmed, and D. Hartmann, 1989: Cloud-radiative forcing and climate: Results from the earth radiation budget experiment. *Science,* **243,** 57–63.

Randerson, J. T., M. V. Thompson, and C. B. Field, 1997: The contribution of terrestrial sources and sinks to trends in the seasonal cycle of atmospheric carbon dioxide. *Global Biogeochem. Cycles,* **11,** 535–551.

Rossow, W. B., and L. C. Gardner, 1993a: Cloud detection using satellite measurements of infrared and visible radiances for ISCCP. *J. Climate,* **6,** 2341–2369.

——, and ——, 1993b: Validation of ISCCP cloud detections. *J. Climate,* **6,** 2370–2393.

Running, S. W., C. O. Justice, and D. Carneggie, 1994: Terrestrial remote sensing science and algorithms planned for EOS/MODIS. *Int. J. Remote Sens.*, **15,** 3587–3602.

Saunders, R. W., and K. T. Kriebel, 1988: An improved method for detecting clear sky and cloudy radiances from AVHRR data. *Int. J. Remote Sens.*, **9,** 123–150.

Schimel, D. S., 1995: Terrestrial ecosystems and the carbon cycle. *Global Change Biol.*, **1,** 77–91.

Schweiger, A. J., and J. R. Key, 1994: Arctic Ocean radiative fluxes and cloud forcing estimated from the ISCCP C2 cloud dataset, 1983–1990. *J. Appl. Meteor.*, **33,** 948–963.

Sellers, P. J., 1987: Canopy reflectance, photosynthesis and transpiration II: The role of biophysics in the linearity of their interdependence. *Int. J. Remote Sens.*, **6,** 1335–1372.

——, and Coauthors, 1995: Modelling the exchanges of energy, water and carbon between continents and the atmosphere. *Science,* **275,** 502–509.

Shao, Y., and A. Henderson-Sellers, 1996: Modeling soil moisture: A project of intercomparison of land-surface parameterization schemes phase 2(b). *J. Geophys. Res.*, **101,** 7227–7250.

Smith, G. L., R. N. Green, E. Raschke, L. M. Avis, J. T. Suttles, B. A. Wielicki, and R. Davies, 1986: Inversion methods for satellite studies of the earth radiation budget: Development of algorithms for the ERBE mission. *Rev. Geophys.*, **24,** 407–421.

Stamnes, K., S. Tsay, W. Wiscombe, and K. Jayaweera, 1988: Numerically stable algorithm for discrete-ordinate method radiative transfer in multiple scattering and emitting layered media. *Appl. Opt.*, **27,** 2502–2509.

Steffen, K., 1987: Bidirectional reflectance of snow at 500–600 nm. *Large Scale Effects of Seasonal Snow Cover: Proceedings of a Symposium held during the XIX Assembly of the International Union of Geodesy and Geophysics at Vancouver, August 1987,* B. E. Goodison, R. G. Barry, and J. Dozier, Eds., IAHS Press, 415–425.

——, 1996: Effect of solar zenith angle on snow anisotropic reflectance. *IRS '96, Current Problems in Atmospheric Radiation: Proceedings of the International Radiation Symposium,* W. L. Smith and K. Stamnes, Eds., A. Deepak Publishing, 1–4.

Stephens, G. L., G. G. Campbell, and T. H. Vonder Haar, 1981: Earth radiation budgets. *J. Geophys. Res.*, **86,** 9739–9760.

Stowe, L., E. McClain, R. Carey, P. Pellegrino, G. Gutman, P. Davis, C. Long, and S. Hart, 1991: Global distribution of cloud cover derived from NOAA/AVHRR operational satellite data. *Adv. Space Res.*, **11,** 51–54.

——, S. Vemury, and A. Rao, 1994: AVHRR clear sky radiation data sets at NOAA/NESDIS. *Adv. Space Res.*, **14,** 113–116.

——, A. M. Ignatov, and R. R. Singh, 1997: Development, validation, and potential enhancements to the second-generation operational aerosol product at the National Environmental Satellite, Data, and Information Service of the National Oceanic and Atmospheric Administration. *J. Geophys. Res.*, **102,** 16 923–16 934.

Stricker, N. C. M., A. Hahne, D. L. Smith, J. Delderfield, M. B. Oliver, and T. Edwards, 1995: ATSR-2: The evolution in its design from ERS-1 to ERS-2. *ESA Bull.*, **83,** 32–37.

Stroeve, J., A. Nolin, and K. Steffen, 1997: Comparison of AVHRR-derived and in-situ surface albedo over the Greenland Ice Sheet. *Remote Sens. Environ.*, **62,** 262–276.

Sud, Y. C., and M. Fennessy, 1982: A study of the influence of surface albedo on July circulation in semi-arid regions using the GLAS GCM. *J. Climatol.*, **2,** 105–125.

Tanre, D., M. Herman, and P. Y. Deschamps, 1983: Influence of the atmosphere on space measurements of directional properties. *Appl. Opt.*, **21,** 733–741.

Taylor, R. V., and L. L. Stowe, 1984: Reflectance characteristics of uniform earth and cloud surfaces derived from *NIMBUS-7* ERB. *J. Geophys. Res.*, **89,** 4987–4996.

Várnai, T., R. Davies, and R. Marchand, 1999: Evaluating cloud albedo retrieval algorithms that use multi-angle radiance measurements. Preprints, *10th Conf. on Atmospheric Radiation*, Madison, WI, Amer. Meteor. Soc., 54–57.

Veefkind, J. P., G. de Leeuw, and P. A. Durkee, 1998: Retrieval of aerosol optical depth over land using two-angle view satellite radiometry during TARFOX. *Geophys. Res. Lett.*, **25,** 3135–3138.

Vermote, E. F., N. El Saleous, C. O. Justice, Y. J. Kaufman, J. L. Privette, L. Remer, J. C. Roger, and D. Tanre, 1997a: Atmospheric correction of visible to middle-infrared EOS-MODIS data over land surfaces: Background, operational algorithm and validation. *J. Geophys. Res.*, **102,** 17 131–17 141.

——, D. Tanre, J. L. Deuze, M. Herman, and J. J. Morcrette, 1997b: Second simulation of the satellite signal in the solar spectrum: An overview. *IEEE Trans. Geosci. Remote Sens.*, **35,** 675–686.

Verstraete, M. M., B. Pinty, and R. B. Myneni, 1996: Potential and limitations of information extraction on the terrestrial biosphere from satellite remote sensing. *Remote Sens. Environ.*, **58,** 201–215.

Walsh, J. E., D. R. Tueck, and M. R. Peterson, 1982: Seasonal snow cover and short-term climate fluctuations over the United States. *Mon. Wea. Rev.*, **110,** 1474–1485.

Wang, M., and H. R. Gordon, 1994: Estimating aerosol optical properties over the oceans with MISR: Some preliminary studies. *Appl. Opt.*, **33,** 4042–4057.

Wanner, W., A. H. Strahler, B. Hu, P. Lewis, J.-P. Muller, X. Li, C. Schaaf, and M. J. Barnsley, 1997: Global retrieval of bidirectional reflectance and albedo over land from EOS MODIS and MISR data: Theory and algorithm. *J. Geophys. Res.*, **102,** 17 143–17 161.

Warren, S. G., 1982: Optical properties of snow. *Rev. Geophys. Space Phys.*, **20,** 67–89.

——, and W. J. Wiscombe, 1980: A model for the spectral albedo of snow, II: Snow containing atmospheric aerosols. *J. Atmos. Sci.*, **37,** 2734–2745.

——, R. E. Brandt, and P. O. Hinton, 1998: Effect of surface roughness on bidirectional reflectance of Antarctic snow. *J. Geophys. Res.*, **103,** 25 789–25 807.

Wessman, C. A., and G. P. Asner, 1998: Ecosystems and the problems of large-scale measurements. *Successes, Limitations, and Frontiers in Ecosystem Ecology*, P. Groffman, and M. Pace, Eds., Springer-Verlag, 346–371.

Wielicki, B. A., B. R. Barkstrom, E. F. Harrison, R. B. Lee III, G. L. Smith, and J. E. Cooper, 1996: Clouds and the Earth's Radiant Energy System (CERES): An Earth Observing System experiment. *Bull. Amer. Meteor. Soc.*, **77,** 853–868.

Winthur, J.-G., 1994: Spectral bi-directional reflectance of snow and glacier ice measured in Droning Maud Land, Antarctica. *Ann. Glaciol.*, **20,** 1–5.